International Journal of Nanomedicine

Dovepress
Taylor & Francis Group

Open Access Full Text Article

ORIGINAL RESEARCH

Injectable Composite Hydrogel Stents for Bone Defect Management with Enhanced Osteogenesis and Angiogenesis

Zhihong Chen[1–3], Mingyu Jia[1,3], Yangyang Liu[1], Huajian Zhou[1,3], Xiaopan Wang[1], Min Wu[1,3]

[1]Department of Orthopedics, The First Affiliated Hospital of Bengbu Medical University, Bengbu Medical University, Bengbu, People's Republic of China; [2]Department of Orthopedics, Fenjinting Hospital in Sihong, Suqian, People's Republic of China; [3]Anhui Province Key Laboratory of Tissue Transplantation, Bengbu Medical University, Bengbu, People's Republic of China

Correspondence: Min Wu; Xiaopan Wang, Department of Orthopedics, The First Affiliated Hospital of Bengbu Medical University, Bengbu Medical University, Bengbu, Anhui, 233004, People's Republic of China, Tel + 86 13865032636; + 86 18715235275, Email wumin197010@163.com; wxpan123@163.com

Background: The use of autologous bone grafting is considered the most successful method for managing bone defects, particularly when utilizing cancellous bone grafts for the best outcomes. Nonetheless, the scarcity of cancellous bone presents a notable obstacle in remedying these defects. Consequently, it is essential to create reliable alternatives to cancellous bone grafts to ensure effective management of bone defects.

Methods: In this research, we created an injectable composite hydrogel stents using gelatin methacrylate (GelMA) hydrogel to mimic the collagen properties of cancellous bone, along with the inclusion of nanohydroxyapatite (nHA) to signify the inorganic element. Furthermore, we incorporated vascular endothelial growth factor (VEGF) to improve regenerative vascular capabilities. Before being implanted into rat cranium defect models, these composite hydrogel stents were co-cultured with human umbilical vein endothelial cells (HUVEC) and bone marrow mesenchymal stem cells (BMSC).

Results: The composite hydrogel stents exhibited a network structure with porosity, robust mechanical properties, and beneficial degradation traits. In the degradation phase, it steadily releases Ca^{2+} and VEGF, which encourages the proliferation, migration, and osteogenic differentiation of BMSCs from rats. Moreover, this release improves the ability of HUVECs to form tubes. Collectively, these mechanisms support the regeneration of blood vessels and bone in the cranium defect region of rats.

Conclusion: The composite hydrogel stents demonstrated excellent cytocompatibility and biological characteristics, as evidenced by its ability to enhance both osteogenesis and angiogenesis in vivo and in vitro. Consequently, it has the potential to act as an effective alternative to natural cancellous bone.

Keywords: nano-hydroxyapatite, vascular endothelial growth factor, laser speckle blood flow imager, bone tissue engineering

Introduction

Bone is a highly vascularized tissue, and blood vessels are essential for bone formation, metabolism, healing, and remodeling.[1] The integrity of bones relies on close spatiotemporal connections between blood vessels and bone cells.[2] Extensive bone defects caused by tumors, trauma, infections, and other factors not only lead to significant damage to bone integrity but also severely compromise the local vascular system. This results in a sharp reduction or complete interruption of blood supply, thereby limiting physiological bone repair.[3] In clinical practice, vascular autologous bone grafting is the standard treatment for a wide range of bone defects. Due to its rich blood supply, this method demonstrates excellent bone repair capabilities.[4] However, it presents challenges such as donor shortages, donor pain, bleeding, and the risk of infection.[5] Allografts and xenografts may pose risks of disease transmission and ethical concerns,[6] and without a sufficient blood supply, the graft failure rate remains high. Bone tissue engineering emerges as a therapeutic strategy aimed at developing bone replacement materials by combining appropriate biomaterials with osteogenic progenitor cells or growth factors. A key challenge in this field is ensuring that the implant effectively promotes both blood vessel regeneration and bone regeneration in vivo.[7]

Received: 2 December 2024
Accepted: 7 April 2025
Published: 12 April 2025

Vascular regeneration is critical for the repair of bone defects, as early vascularization enhances the supply of nutrients and oxygen, and facilitates the recruitment of stem cells and growth factors to the defect area,[8] such as vascular endothelial growth factor (VEGF)[9] and platelet-derived growth factor (PDGF).[10] The subsequent formation of a vascular network is essential for providing ions necessary for bone tissue mineralization.[11] Inhibition of angiogenesis during the repair of bone defects can result in the formation of fibrous scar tissue, which may lead to bone nonunion.[12] VEGF serves as a key regulator of physiological angiogenesis during both embryonic development and postnatal life; it increases the permeability of blood vessels and promotes the functionalization of endothelial cells.[13] Additionally, VEGF can stimulate the sprouting of pre-existing peripheral blood vessels into the bone defect area, contributing to the formation of bone repair tissue.[14] Recent studies have demonstrated that elevating VEGF levels in osteoblasts can enhance both vascular and bone regeneration.[15] Beyond its role in angiogenesis, VEGF also influences the maturation and ossification of osteoblasts.[16] However, excessively high local concentrations of VEGF may lead to vascular hyperplasia, potentially causing complications such as vascular malformations and increased recruitment of osteoclasts, which can result in bone resorption. Therefore, the development of a tissue engineering system for the low-concentration, site-directed sustained release of VEGF is essential to achieve a balance between vascular regeneration and bone regeneration.

Hydroxyapatite (HA) is the primary mineral component of human bone tissue, exhibiting favorable properties such as bone conduction, osteoinduction, and cell adhesion.[17] Nanoscale hydroxyapatite (nHA) resembles the microstructure of human bone tissue and demonstrates excellent osteogenic capability and biocompatibility. Furthermore, the reduction in nHA particle size results in a larger specific surface area, enabling its use as a drug carrier for targeted delivery to bone tissue.[18] However, due to the high brittleness and powdery nature of nHA, its application as a standalone material for bone reconstruction is challenging. To address this limitation, researchers have combined nHA with various materials, including both natural and synthetic organic substances, to create composite biomaterials that enhance its biological properties.[19–21] Certain hydrogels have been demonstrated to bind with calcium phosphate compounds, facilitating in vitro self-mineralization,[22] and serve as drug carriers for targeted, low-concentration drug release,[23] thus finding widespread application in tissue engineering. GelMA hydrogels are synthesized by incorporating methacrylate groups into the amino groups of gelatin,[24] preserving the RGD sequence that promotes cell migration, adhesion, and differentiation.[25] Additionally, these hydrogels can be combined with calcium ions to achieve mineralization. Their three-dimensional porous structure is capable of accommodating various drug molecules, enabling targeted delivery. Research indicates that 5% (w/v) GelMA hydrogels effectively promote the osteogenic differentiation of bone marrow mesenchymal stem cells,[26] enhancing their utility in bone tissue engineering. Lu et al utilized exosome-loaded GelMA-nHA hydrogels to achieve slow, site-directed release of exosomes, thereby promoting vascular and bone regeneration in the skull defect area of rats.[27]

In this study, an injectable composite hydrogel was prepared by combining VEGF, nHA, and GelMA through UV light cross-linking. The composite hydrogel demonstrated drug-loading capability and a low-concentration slow-release ability, facilitating the gradual release of VEGF and calcium ions, thereby achieving a synergistic effect on vascular and bone regeneration. Bone marrow mesenchymal stem cells (BMSCs) were inoculated onto the composite scaffold to evaluate its performance in promoting cell adhesion, proliferation, and osteogenic differentiation. Concurrently, the scaffold enhanced the tubular formation of human umbilical vein endothelial cells (HUVECs). Furthermore, to investigate the bone and vascular regeneration potential of the composite scaffold, it was applied to repair rat skull defects with a diameter of 5 mm. The results indicated that the composite scaffold significantly improved the regenerative effects on both bone and blood vessels in the bone defects. In conclusion, the successful preparation of composite hydrogel stents and their effective performance in promoting bone and blood vessel regeneration offer a promising approach for the treatment of bone defects in tissue engineering.

Materials and Methods

Materials

Gelatin methacryloyl (GelMA), nano-hydroxyapatite (nHA), and the photoinitiator were procured from Aladdin Company (Shanghai, China). VEGF was obtained from MCE Corporation (USA. Additionally, Dulbecco's Modified Eagle Medium (DMEM), the Modified Eagle Medium Nutrient Mixture F-12 (DMEM/F12), along with fetal bovine serum (FBS), were obtained from Gibco located in the USA.

Preparation of Composite Hydrogel Scaffold

Different concentrations of VEGF and nHA were mixed with GelMA and co-cultured with BMSCs. After three days, the proliferation ability of BMSC cells at varying concentrations of VEGF and nHA was assessed using the CCK-8 method, leading to the selection of the lowest concentration of both nHA and VEGF for this study.

First, 100 mg of GelMA and 0.5 mg of a photoinitiator were dissolved in 2 mL of phosphate-buffered saline (PBS) in a water bath maintained at 60 °C while away from light. The solution was then allowed to cool to room temperature. Second, 20 mg of nHA and 0.2 μg of VEGF were introduced into GelMA hydrogel, mixing them ultrasonically for 5 seconds. The resulting composite hydrogel (80 μL) was transferred into a solidification ring and exposed to 405 nm wavelength UV light for 30 seconds to facilitate cross-linking, thus yielding a GelMA/nHA/VEGF composite hydrogel scaffold. The procedures for synthesizing GelMA and GelMA/nHA hydrogels are the same as previously outlined.

Characterization of Composite Hydrogel Scaffold

Composite hydrogel scaffolds prepared from GelMA, GelMA/nHA, and GelMA/nHA/VEGF were freeze-dried and made brittle by exposure to liquid nitrogen before being coated with a layer of gold. The morphology of these hydrogels was analyzed using scanning electron microscopy (SEM) and elemental energy spectrum analysis. Water contact angles were measured with a contact angle analyzer, while the pressure-strain characteristics of the hydrogels were evaluated using a universal testing machine, which simultaneously assessed compressive length and load. Strain and stress were calculated according to the formulas provided below:

$$\text{Strain} = \frac{L_0 - L_1}{L_0} \times 100\% \qquad \text{Stress} = \frac{P}{A} \times 100\%$$

L_0 and L_1 represent the initial height of the sample and the height of the sample at different time points, respectively; P and A represent compressive load and cross-sectional area of the hydrogel, respectively.

The degradability of the composite hydrogel was assessed in phosphate-buffered saline (PBS) through a gravimetric approach. Briefly, the hydrogel was placed in PBS buffer (pH = 7.4), then removed at predetermined time intervals. Any surface moisture was blotted away before weighing. The formula used to calculate the degradation rate is as follows:

$$\text{Degradation rate} = \frac{W_0 - W_1}{W_0} \times 100\%$$

W_0 and W_1 represent the initial weight of the sample and the weight of the sample at different time points.

An inductively coupled plasma (ICP) device (Agilent, 5100 SVDV, USA) was used to assess the release of calcium ions (Ca2+). An enzyme-linked immunosorbent assay (ELISA) was utilized to quantify VEGF release. A 1 mL sample of GelMA/nHA/VEGF hydrogel underwent photo-cross-linking, then immersed in a PBS solution. Periodic aliquots were taken from the solution to evaluate the quantity of VEGF released for determining the cumulative release percentage.

In vitro Cytocompatibility of Composite Hydrogel Scaffold

Cell Culture

The BMSCs were isolated and cultured following established protocols.[28] Specifically, BMSCs were obtained from the femoral bone marrow of 4-week-old Sprague-Dawley (SD) rats and cultured in DMEM/F12 medium supplemented with 1% penicillin/streptomycin and 10% fetal bovine serum (FBS), with the medium refreshed every three days. For in vitro experiments, cells from passages three to five were used. Additionally, HUVECs were maintained in DMEM medium supplemented with 1% penicillin/streptomycin and 10% FBS, with the medium also changed every three days.

Cell Proliferation, Adhesion, and Migration Abilities

BMSCs were placed into 96-well plates at a density of 8000 cells per well and were co-cultured with different hydrogel scaffolds for durations of 1, 2, and 3 days. To evaluate the viability of cells, a cell counting kit (CCK-8) purchased from Beyotime (Shanghai, China), was utilized. The absorbance (optical density values) was recorded at a wavelength of 450 nm with the help of a microplate reader.

BMSCs were inoculated into 24-well plates at a concentration of 3×10^4 cells per well and cultured with different hydrogel scaffolds for 1, 3, and 5 days. To assess the viability of cells, a dual staining kit specifically for live and dead cells (Solaibao, Shanghai, China) was used, incorporating calcein-AM at a concentration of 2 μM and propidium iodide (PI) at 5 μM. The samples were incubated for 15 minutes at 37 °C, in darkness. Images were taken using an inverted fluorescence microscope.

BMSCs were seeded in a 6-well plate at a density of 1.0×10^5 cells per well and allowed to incubate for 24 hours. To create parallel lines on the well plate's surface, a 200 μL pipette tip was used. The culture medium was then replaced with a 2% low-serum solution, and the cells were co-cultured with the hydrogel scaffold for 36 hours. After incubation, the cells were stained with 2 μM calcein for 15 minutes. Observations were performed using an inverted fluorescence microscope.

BMSCs were plated in 24-well plates at a density of 3×10^4 cells per well and cultured with various hydrogel scaffolds for 5 days. After this period, the cells were fixed using 4% paraformaldehyde for 15 minutes and subsequently treated with FITC-conjugated phalloidin for 30 minutes to visualize F-actin. Following this, the cells were stained with 6-diamidino-2-phenylindole (DAPI) for 15 minutes. The cells were then washed with PBS for 5 minutes per wash. Images were captured using an inverted fluorescence microscope.

In vitro Osteogenic Ability of Composite Hydrogel Scaffold

BMSCs were cultured in 6-well plates at a density of 8×10^4 cells per well. Once the cells reached 70% confluence, the culture medium was switched to osteogenic medium, and the cells were co-cultured with various hydrogel scaffolds for 7 days. To quantify alkaline phosphatase (ALP) activity in the culture supernatants, a detection kit from Beyotime (Shanghai, China) was employed. Cells adhering to the wells were fixed with 4% formaldehyde for 15 minutes and subsequently stained to assess ALP activity. On day 21, the cells underwent alizarin red staining (ARS, Beyotime, Shanghai, China) to evaluate mineralization, and observations were made using an inverted fluorescence microscope. BMSCs were seeded in 24-well plates at a density of 3×10^4 cells per well. Once the cells reached approximately 70% confluence, the growth medium was replaced with osteogenic medium, and the cells were subsequently cultured on the composite hydrogel scaffold. Fluorescent staining for RUNX-2 and osteocalcin (OCN) was performed on days 7 and 21, respectively. To fix the cells, they were treated with a 4% paraformaldehyde solution for 15 minutes, followed by a 15-minute incubation with 0.3% Triton X-100. For blocking, the cells were incubated with goat serum for 2 hours. They were then exposed to primary antibodies specific to RUNX-2 (1:100, Affinity, Jiangsu, China) and OCN (1:100, Affinity, Jiangsu, China) at 4 °C overnight. After washing, the cells were incubated for 2 hours with a fluorescently labeled secondary antibody (goat anti-rabbit IgG CY3-conjugated, Affinity, S0011, Jiangsu, China), followed by a 15-minute DAPI staining. Finally, images were captured using an inverted fluorescence microscope.

In vitro Angiogenic Ability of Composite Hydrogel Scaffold

BMSC cells were seeded in 24-well plates at a density of 3×10^4 cells per well and incubated for 3 days. Hydrogel scaffolds were then placed in the upper chamber and co-cultured with the BMSCs for an additional 3 days. After this co-culture period, the cells were fixed using 4% paraformaldehyde for 15 minutes, followed by permeabilization with 0.3% Triton X-100 for 15 minutes. The cells were then blocked with 10% goat serum for 2 hours. Subsequently, they were incubated with a primary antibody specific to CD31 (1:100, Affinity, Jiangsu, China) at 4 °C overnight. The cells were then rinsed and exposed to a fluorescently labeled secondary antibody (Goat Anti-Rabbit IgG CY3-conjugated, Affinity, S0011, Jiangsu, China) for 2 hours. DAPI was utilized for nuclear staining and incubated for 15 minutes. Images were obtained using an inverted fluorescence microscope.

A total of 100 μL of Matrigel was added to the bottom of a 24-well plate and incubated at 37 °C for 30 minutes. The HUVECs were then seeded onto the Matrigel layer at a density of 1.5×10^5 cells per well and co-cultured with the hydrogel scaffold for 6 hours. Following this incubation period, the cells were stained with calcein (2 μM) for 15 minutes and visualized using an inverted fluorescence microscope.

In vivo Osteogenic and Angiogenic Ability of Composite Hydrogel Scaffold

Establishment of Animal Models

Male Sprague-Dawley (SD) rats were obtained from Jiangsu Nanjing Wukong Biotechnology Co., Ltd. (Nanjing, China). These eight-week-old rats weighed approximately 280 g and were randomly assigned to one of four groups: control, GelMA, GelMA/nHA, and GelMA/nHA/VEGF. Anesthesia was induced via an intraperitoneal injection of sodium pentobarbital (50 mg/kg). The cranial area was then shaved and disinfected. Using an electric drill, a bone defect measuring 5 mm in diameter was created on each side of the cranial suture. A hydrogel was shaped into a stent (5 mm in diameter and 1 mm in height) and implanted into the defect site, secured in place with sutures. The muscle and skin layers were then stitched together. Data collection and sampling were conducted at both 4 and 8 weeks post-surgery.

Imaging

A laser speckle flow imager (Reward, Shenzhen, China) was utilized to assess blood flow in the area of the skull defect at 4 and 8 weeks to gather imaging data. The rats were then euthanized through carbon dioxide asphyxiation. The skulls were collected and preserved in a 4% paraformaldehyde solution for 24 hours. The samples were then examined using Micro-CT, followed by three-dimensional reconstruction to analyze the healing potential of the bone defect.

Tissue Staining

The skull specimens were decalcified, embedded in paraffin, and then sliced into 7 μm thick sections. Standard staining techniques, including hematoxylin and eosin (H&E) and Masson's trichrome stain, were applied to these sections for histological evaluation. In addition, immunofluorescence staining was performed to target platelet endothelial cell adhesion molecule (CD31), α-smooth muscle actin (α-SMA), osteocalcin (OCN), and runt-related transcription factor 2 (RUNX-2). An inverted fluorescence microscope facilitated the imaging of the samples, while ImageJ software was utilized for the quantitative analysis of the fluorescence results.

Statistical Analysis

The data are presented as means and standard deviations. All statistical analyses were conducted using Origin and GraphPad Prism version 9.5.1. To assess the experimental data among different groups, a one-way analysis of variance (ANOVA) was utilized. A p-value below 0.05 was considered statistically significant.

Results

Composite Hydrogel Scaffold Characterization

CCK-8 results showed that the concentrations of BMSCs co-cultured with nHA and VEGF were 2.5mg/mL and 100ng/mL respectively (Figure S1,2). The liquid hydrogel gradually transitioned into a gel when exposed to ultraviolet light at a wavelength of 405 nm (Figure 1A). Scanning electron microscopy (SEM) demonstrated that all samples showed a loose and interconnected porous architecture. Importantly, nHA increased the roughness of the pore surfaces and reduced pore sizes. Energy spectrum analysis revealed that both nHA and VEG were distributed across the pore surfaces (Figure 1B). Figure C shows the content of each group of elements. The composite hydrogel bone scaffold exhibited a swift release of vascular endothelial growth factor (VEGF) during the first week, attaining a release rate of 33.2%. Following this period, the release rate progressively declined, leading to an accumulated release total of 59.8% (Figure 1D). Conversely, the release of Ca2+ rose consistently during the initial 14 days before leveling off (Figure 1E). Interestingly, there was no significant difference in release rates between the two groups. The mechanical properties of the composite hydrogel with nHA and VEGF were considerably better than those of the plain GelMA group (Figure 1F and G, $p < 0.05$). The high hydrophilicity of a hydrogel scaffold is crucial for promoting cell adhesion. The water contact angle of the composite hydrogel steadily decreased (Figure 1H). The uniform distribution of nHA across the pore surfaces of the composite hydrogel enhanced its structural stability, thus decreasing the hydrogel's degradation rate (Figure 1I).

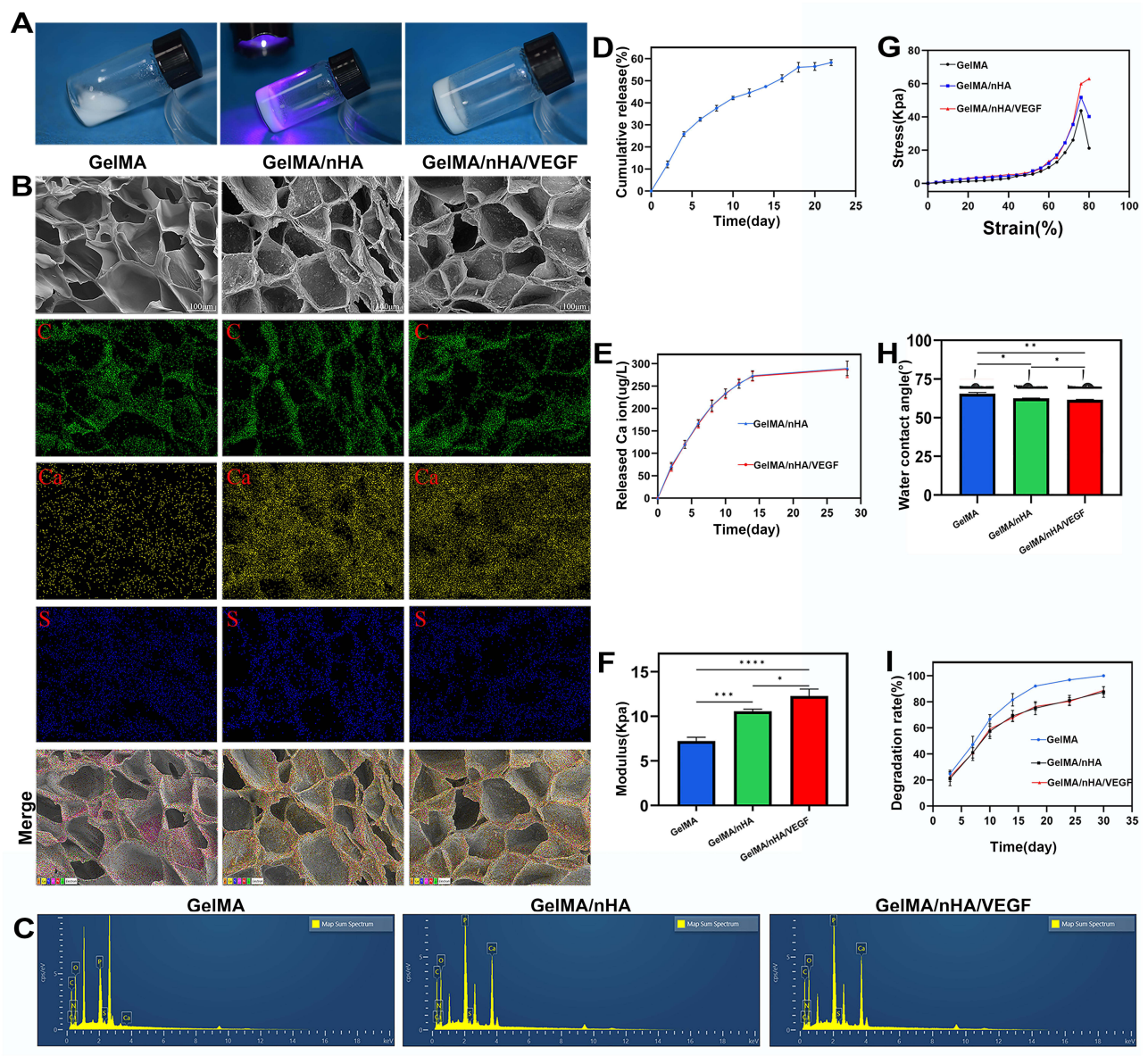

Figure 1 Characterization of the hydrogel scaffolds. (**A**) Illustration of hydrogel gel properties. (**B**) Scanning electron microscope images and energy dispersive spectroscopy analysis images showing the cross-sections of hydrogel scaffolds in each group at 5000X magnification. (**C**) The content of each group of elements. (**D**) The sustained release curve of VEGF in hydrogel scaffolds. (**E**) The sustained release curve of Ca^{2+} in hydrogel scaffolds. (**F**) Compressive modulus. (**G**) Stress-strain curve of hydrogel scaffolds. (**H**) A chart of water contact angles of hydrogel scaffolds in the indicated groups. (**I**) The degradation curves of hydrogel scaffolds in the indicated groups. (C) Carbon element. Ca: Calcium element. (S) Sulfur element. Data are shown as mean ± SD. (n≥3); ns.: no significant, *: $p< 0.05$, **: $p< 0.01$, ***: $p< 0.001$, ****: $p< 0.0001$.

In vitro Cytocompatibility of Composite Hydrogel Scaffold

The biocompatibility of the biomimetic hydrogel scaffolds was assessed by examining key factors such as cell proliferation, viability, and adhesion. Cell viability was determined using live/dead staining, which showed that cells in all experimental groups remained healthy throughout the 5-day culture period. This indicates that the hydrogel scaffold supports the extended survival of BMSCs, as illustrated in Figure 2A and B. To evaluate cell migration, an in vitro scratch assay was performed. Notably, the GelMA/nHA/VEGF group demonstrated enhanced adhesion and migration capabilities after 36 hours of scratching compared to the other groups. Quantitative analysis of the scratched areas further validated the fluorescence results (Figure 2C and D). Fluorescence staining techniques were utilized to examine the morphology and extension of the cytoskeleton and nucleus on the 5th day of culture. The cytoskeleton was distinctly observable across all groups, with the GelMA/nHA/VEGF group exhibiting the most significant extension and the

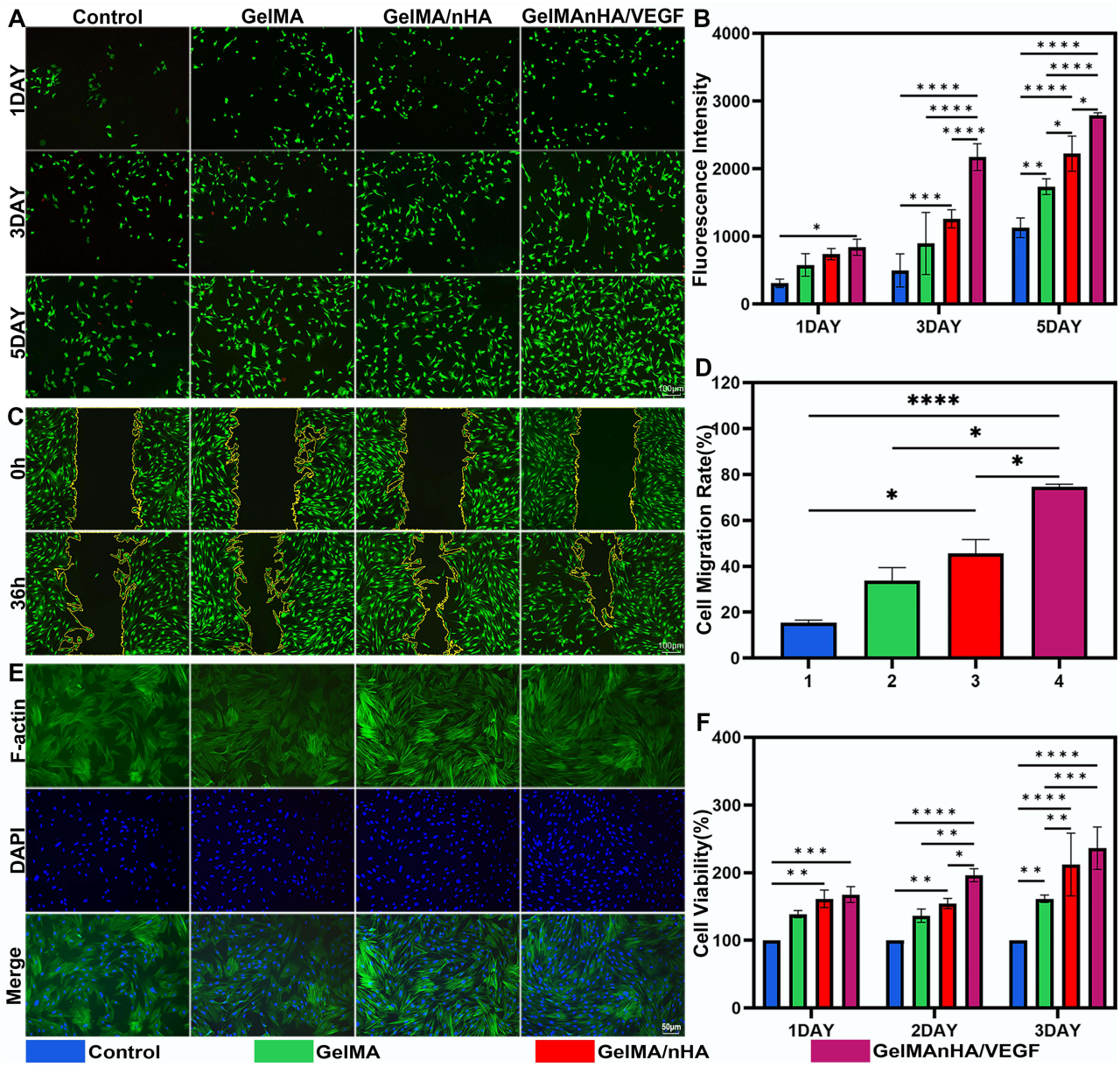

Figure 2 In vitro biocompatibility analyses. (**A**) Calcein-AM staining of BMSCs following co-incubation with different groups for 1, 3, and 5 days. (**B**) Semi-quantitative analysis of cell viability, as determined by the live/dead assay. (**C**) The migration ability of BMSCs evaluated the scratch test. (**D**) Quantitative analysis of cell migration rate. (**E**) Cytoskeleton staining displaying the BMSCs after co-culture with hydrogel scaffolds. (**F**) The CCK-8 values. Data are shown as mean ± SD. (n≥3); ns.: no significant, *: $p< 0.05$, **: $p< 0.01$, ***: $p< 0.001$, ****: $p< 0.0001$.

highest capacity for cell proliferation (Figure 2E), consistent with the findings from the live/dead staining. Cell proliferation was measured using the CCK-8 assay, and the results were consistent with those from the live/dead staining (Figure 2F).

In vitro Osteogenic Ability of Composite Hydrogel Scaffold

The initial osteogenic properties of the hydrogel scaffold were evaluated by assessing the activity of ALP and RUNX-2. ALP staining revealed a significant increase in ALP activity in the GelMA/nHA/VEGF group compared to the other experimental groups after seven days of culturing BMSCs with the hydrogel scaffold (Figures 3A). Additionally, fluorescence staining showed that RUNX-2 activity, a protein that plays a crucial role in the early stages of osteoblast differentiation, was significantly higher in the GelMA/nHA/VEGF group compared to the other groups (Figures 3B).

https://doi.org/10.2147/IJN.S509686

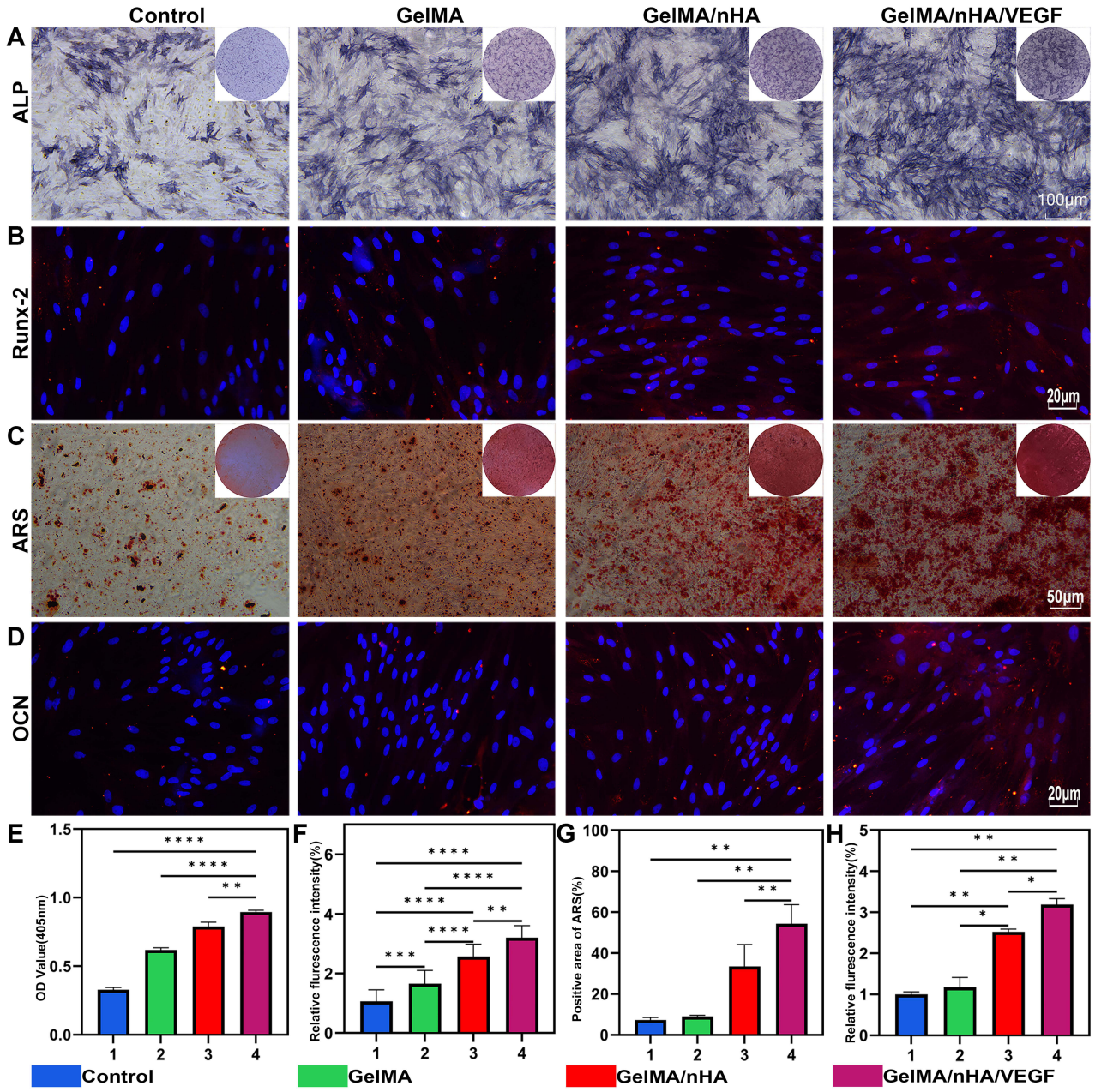

Figure 3 The capacity for bone induction in composite hydrogel scaffolds. (**A**) The ALP staining results after 7 days of bone marrow mesenchymal stem cells culture showed that the GelMA/nHA/VEGF group had the strongest expression. (**B**) Fluorescence microscopy images of Runx-2 across each group after the 7-day co-culture with hydrogel scaffolds and BMSCs. (**C**) After 21 days of co-culturing bone marrow mesenchymal stem cells (BMSCs) with hydrogel scaffolds, Alizarin red staining of BMSCs showed more osteoid tuberculosis and calcium deposition in the GelMA/nHA/VEGF group. (**D**) Fluorescence microscopy images of OCN in specified groups after 21 days of co-culture involving hydrogel scaffolds and BMSCs. (**E**–**H**) Quantitative analysis of expression levels of ALP, Runx-2, ARS and OCN showed that the osteogenic differentiation of the GelMA/nHA/VEGF group was better than that of other groups. Data is presented as mean ± SD (n≥3); ns.: not significant, *: $p< 0.05$, **: $p< 0.01$, ***: $p< 0.001$, ****: $p< 0.0001$.

Calcium nodules are typically formed during the later stages of osteoblast maturation. In the present study, Alizarin red staining (ARS) was utilized to examine the impact of the hydrogel scaffold on the osteogenic differentiation of BMSCs over a span of 21 days. The results revealed a substantial rise in the density of calcium nodules in the group of BMSCs cultured with GelMA/nHA/VEGF, signifying improved osteogenic activity (Figures 3C). Osteocalcin (OCN), which is mainly secreted by osteoblasts, plays a crucial role in the regulation of calcium metabolism in bones. After 21 days of BMSC induction, immunofluorescence images of OCN were consistent with RUNX-2 results (Figure 3D). We utilized

the alkaline phosphatase detection kit to assess ALP levels in the medium supernatant, revealing that the ALP content in the GelMA/nHA/VEGF group was the highest (Figure 3E). The fluorescence quantitative analysis of RUNX-2 corroborates the results observed microscopically (Figure 3F). Similarly, the positive area results of ARS align with the microscopic observations (Figure 3G). Furthermore, the fluorescence quantitative analysis of OCN also corresponds with the microscopic findings (Figure 3H). These results indicate that the hydrogel scaffold possesses osteogenic properties, particularly enhanced by the synergistic effects of nHA and VEGF, which demonstrate a stronger osteogenic capability. Consequently, the hydrogel scaffold may serve as a foundation for in vivo experiments aimed at further evaluating its osteogenic potential.

In vitro Angiogenic Ability of Composite Hydrogel Scaffold

BMSCs can differentiate in multiple directions and convert into endothelial cells when stimulated with VEGF. Herein, the marker CD31, primarily found in endothelial cells, was utilized to assess how effectively the composite hydrogel scaffold could facilitate the differentiation of BMSCs into endothelial cells. Results from immunofluorescence staining indicated that the expression levels of CD31 were markedly higher in the GelMA/nHA/VEGF group than in the control group (Figure 4A). Meanwhile, tubule formation assays were conducted to evaluate the effect of composite hydrogel scaffolds on the angiogenic potential of HUVECs (Figure 4B). Additionally, we performed quantitative analyses of CD31 (Figure 4C), tubule length (Figure 4D), and the number of nodes (Figure 4E). The GelMA/nHA/VEGF group demonstrated a significant ability to enhance angiogenesis.

In vivo Osteogenic Ability of Composite Hydrogel Scaffold

The scaffold was placed in a rat skull defect model to further assess the osteogenic capabilities of the composite hydrogel scaffold in vivo. The samples were obtained at 4 and 8 weeks to evaluate bone growth through CT scanning and perform quantitative analyses. Notably, no postoperative inflammation or complications were observed at the wound site. Three-dimensional reconstructions via computed tomography (CT) indicated that bone regeneration was restricted in the control group, with new bone primarily forming around the edges of the defect and lacking bony connections in the central region. In contrast, new bones were formed in the group treated with the hydrogel scaffold. Besides, the addition of nano-hydroxyapatite (nHA) promoted the establishment of bony connections within the center of the defect. Importantly, new bone formation was significant in the GelMA/nHA/VEGF group, with the defect area nearly fully regenerated by new bone at the 8-week. Quantitative analysis showed similar results (Figure 5A–C).

Histological assessments were performed using H&E staining and Masson's trichrome staining to analyze the development of new bone in the area of the defect. H&E staining revealed that bone formation was evident in the defect areas across all groups. However, mainly fibrous tissue filled the defect areas in the blank group. In contrast, significant new bone growth occurred in the hydrogel-implanted group, especially in the GelMA/nHA/VEGF bone. The new bone progressed along the scaffold's surface towards the defect center in the GelMA/nHA/VEGF groups (Figure 5D). Similarly, Masson's trichrome staining confirmed an increase in new bone formation within the defect region (Figure 5E). An immunofluorescence analysis was performed in the 4th and 8th week to examine the osteogenic characteristics of the hydrogel in vivo and the expression levels of osteogenic markers, particularly osteocalcin (OCN) and runt-related transcription factor 2 (RUNX-2) (Figure 6A and B). OCN protein staining results across all groups displayed a steady increase of the expression levels over time, as shown by quantitative analysis (Figure 6C and D). RUNX-2 is a vital transcriptional regulator that directs osteogenic differentiation and directly or indirectly affects the expression of genes specific to osteoblasts. In this research, the expression levels of the RUNX-2 protein were notably elevated in the GelMA/nHA/VEGF group during the 4th week when compared to the other groups (Figure 6E). In contrast, RUNX-2 expression decreased in the GelMA/nHA/VEGF group in the 8th week compared with (Figure 6F).

In vivo Angiogenic Ability of Composite Hydrogel Scaffold

A sufficient blood supply is crucial for the repair of bone tissue. In this study, blood flow in the area of the skull defect and the expression levels of CD31 and α-SMA were evaluated to assess how effectively the hydrogel scaffold facilitates the formation of blood vessels. Blood flow was no significantly different between the blank and GelMA groups in the 4th

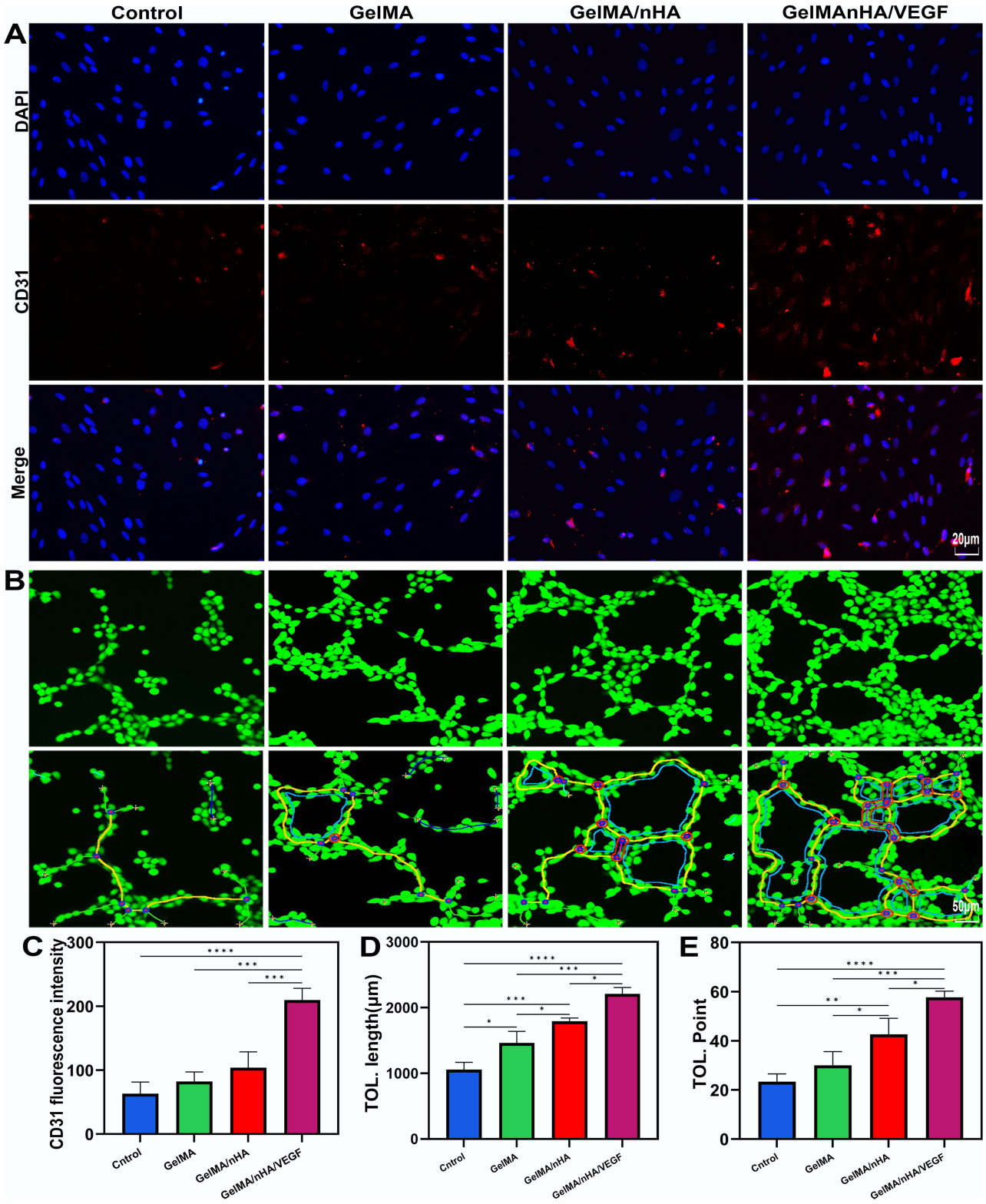

Figure 4 In vitro studies on angiogenesis. (**A**) Immunofluorescence images depicting BMSCs co-cultured with composite hydrogel scaffolds, where the nucleus is colored blue and CD31 appears in red. (**B**) Tube formation in HUVECs after a 6-hour culture across the specified groups. (**C**) Quantitative analysis of CD31. (**D** and **E**) Statistical assessment of the tubes formed in the specified groups after 6 hours of co-culture. Results are presented as mean ± SD (n≥3); ns.: not significant, *: $p< 0.05$, **: $p< 0.01$, ***: $p< 0.001$, ****: $p< 0.0001$.

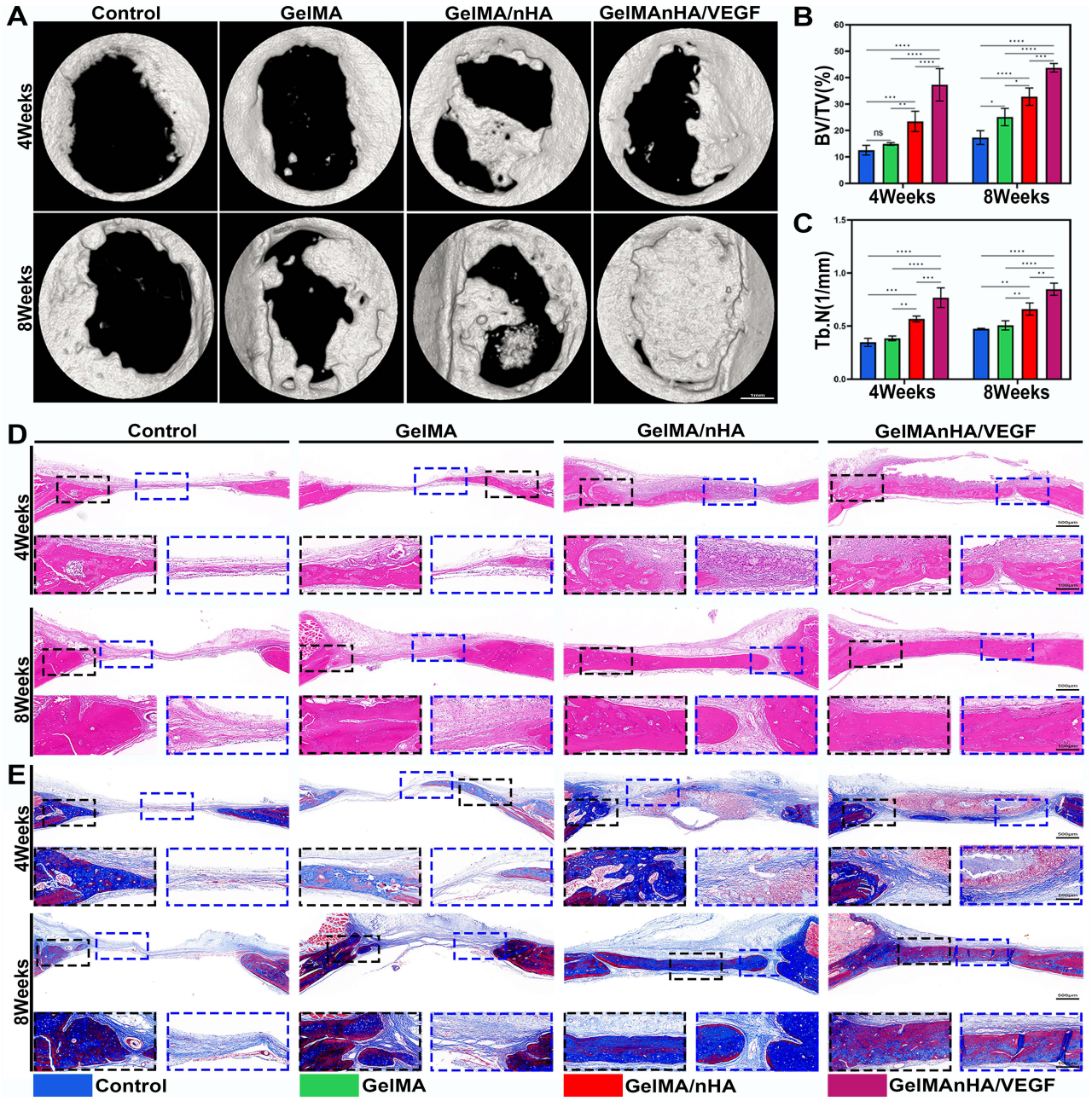

Figure 5 Assessment of bone regeneration in vivo. (**A**) 3D micro-CT images of rat skulls, illustrating changes after 4 and 8 weeks of treatment. (**B** and **C**) Quantitative analysis showing BV/TV and the number of trabecular bones at the defect sites. (**D**) H&E-stained images representing the defect areas in the specified groups after treatment durations of 4 and 8 weeks. (**E**) Masson-stained images of the same defect regions in the specified groups post-treatment at 4 and 8 weeks. The data are presented as mean ± SD. (n≥3) ns.: not significant, *: $p< 0.05$, **: $p< 0.01$, ***: $p< 0.001$, ****: $p< 0.0001$.

week. Notably, the blood flow was significantly increased in the GelMA/nHA and GelMA/nHA/VEGF groups, especially in GelMA/nHA/VEGF group. The bone in the GelMA/nHA/VEGF group had substantially healed in the 8th week, with a decline in blood flow (Figures 7A). The fluorescence staining of tissue sections was largely consistent with the blood flow imaging results. At 4 weeks, CD31 expression was the highest (Figure 7B). By 8 weeks, the blood vessels in the GelMA/nHA/VEGF group were remodeled following the healing of the bone defect area, which led to a decrease in α-SMA expression (Figure 7C). The quantitative analysis of blood flow dynamics at 4 and 8 weeks (Figure 7D and E) was also largely consistent with the imaging results. Furthermore, the quantitative analysis of CD31 and α-SMA aligned with the staining results (Figure 7F and G).

https://doi.org/10.2147/IJN.S509686

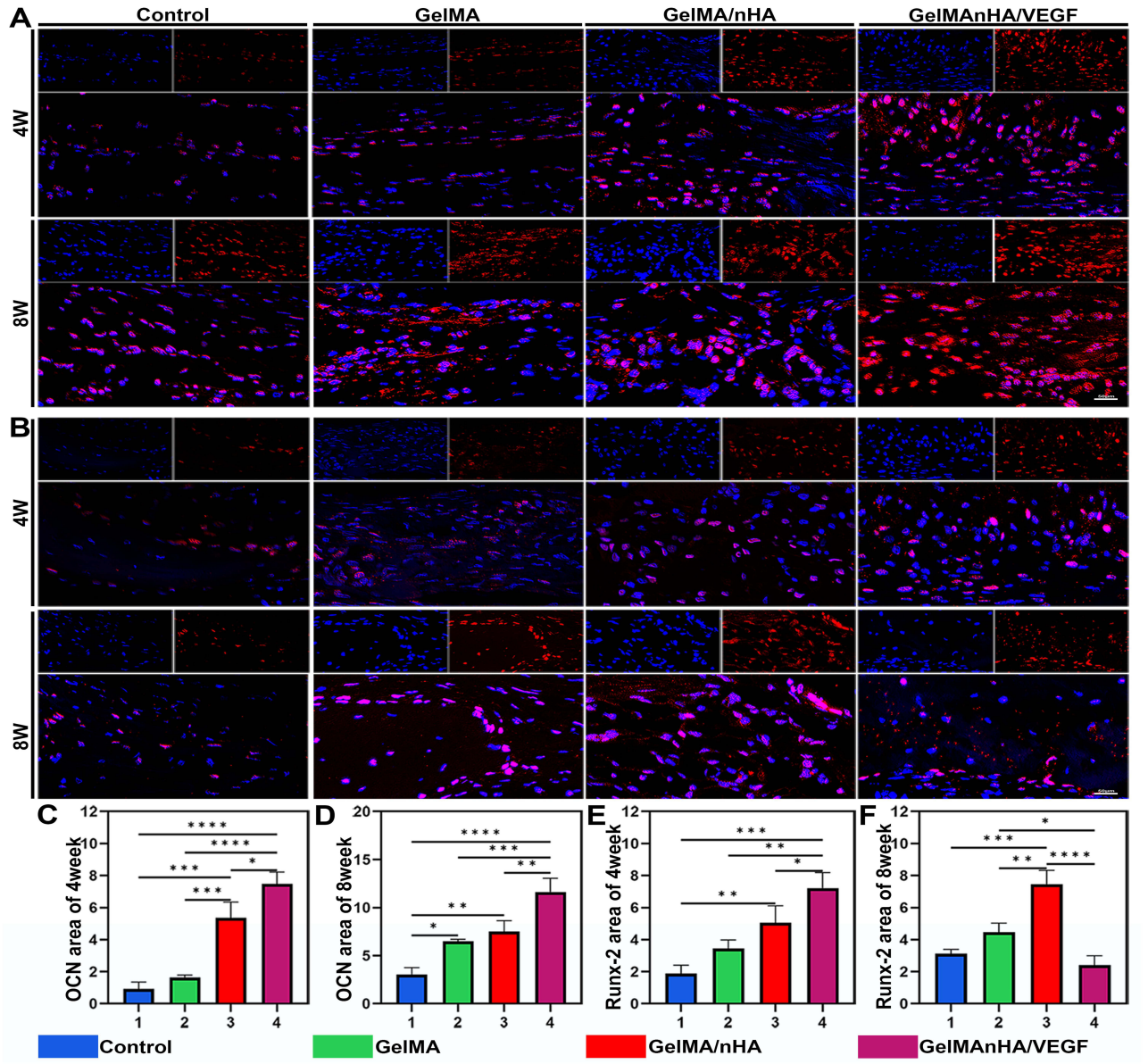

Figure 6 In vivo osteogenesis evaluation. (**A** and **B**) Immunofluorescent staining of OCN, Runx-2 at 4 and 8 weeks. (**C** and **D**) Quantitative analyses of OCN at 4 and 8 weeks. (**E** and **F**) Quantitative analyses of Runx-2 at 4 and 8 weeks. Data are shown as mean± SD. (n≥3); n.s.: no significant, Data are shown as mean± SD. (n≥3); ns.: no significant, *: $p< 0.05$, **: $p< 0.01$, ***: $p< 0.001$, ****: $p< 0.0001$.

Discussion

The rapid development of bone tissue engineering offers an innovative strategy for addressing bone defects. Hydrogels, particularly injectable hydrogels, have gained prominence in this field due to their ability to conform to various defect shapes using hollow needles or catheters, facilitating the distribution of bioactive molecules within the bone defect area.[29] However, these hydrogels typically exhibit low mechanical strength and poor fatigue resistance, which have been key concerns for researchers. To enhance mechanical properties, a variety of organic and inorganic fillers, including ceramics, metals, and bioactive glasses, have been integrated into hydrogel networks to create composite materials with superior mechanical characteristics.[30] In this experiment, we utilized GelMA hydrogel as the organic component and nHA as the inorganic component, incorporating VEGF to produce a composite hydrogel scaffold through simple physical mixing, ultrasonic mixing, and ultraviolet cross-linking. This study demonstrates that the inclusion of nHA enhances the mechanical properties of GelMA.

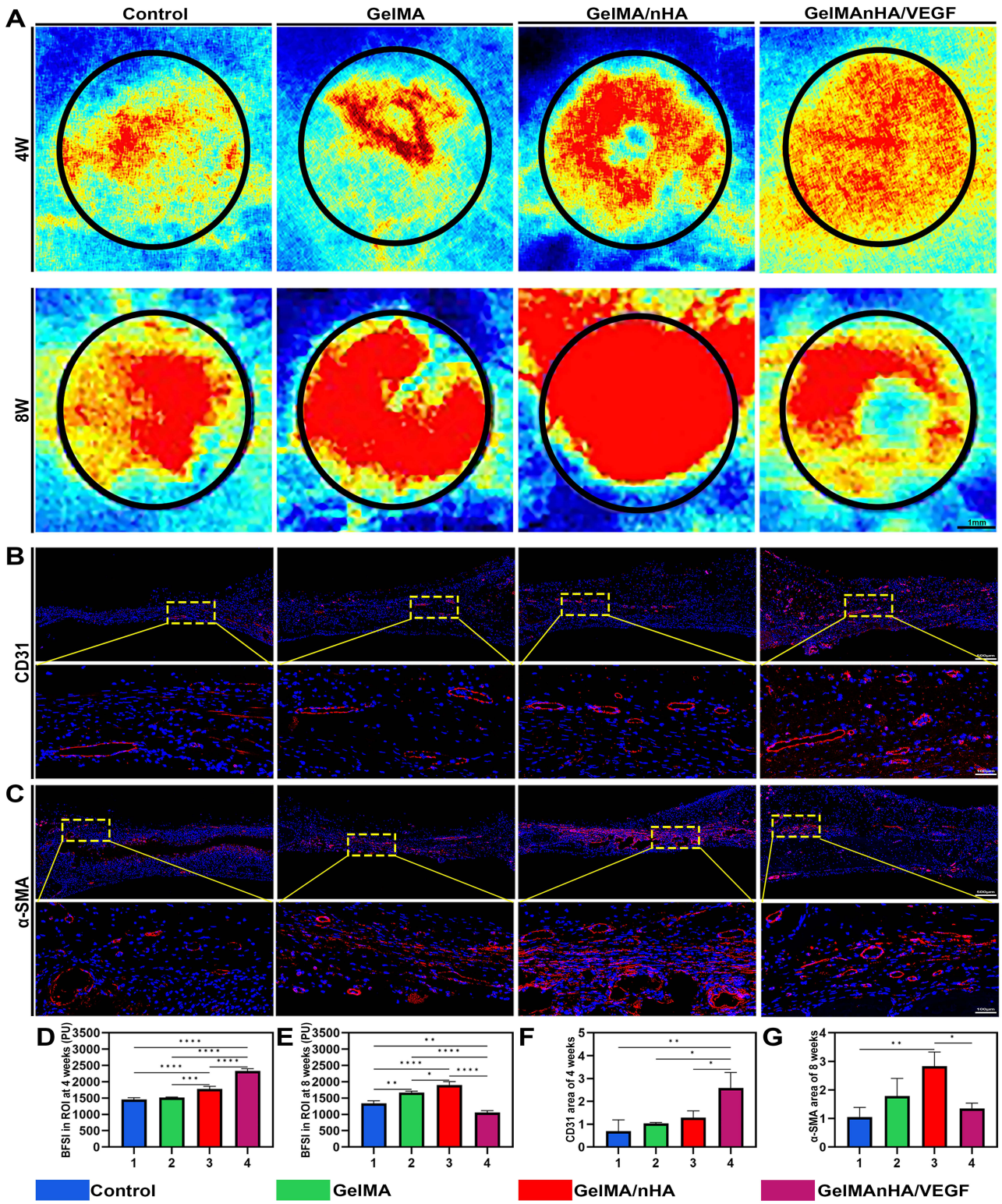

Figure 7 In vivo angiogenesis evaluation. (**A**) Representative images of BFSI by LSCI in different groups at different time points. (**B**) Immunofluorescent staining of CD31 at 4 weeks. (**C**) Immunofluorescent staining of α-SMA at 8 weeks. (**D** and **E**) Quantitative analysis of blood flow changes in bone defect areas at the indicated time points. (**F**) Quantitative analyses of CD31 at 4 weeks. (**G**) Quantitative analyses of α-SMA at 8 weeks. Data are shown as mean± SD. (n≥3); n.s.: no significant, Data are shown as mean± SD. (n≥3); ns.: no significant, *: $p< 0.05$, **: $p< 0.01$, ***: $p< 0.001$, ****: $p< 0.0001$.

https://doi.org/10.2147/IJN.S509686

The characterization of the composite scaffold reveals that nHA and VEGF are distributed within the pores of the hydrogel. However, due to differences in physical and chemical properties during the mixing process, as well as the limitations of gelation conditions, nHA and VEGF may not achieve uniform distribution. Nonetheless, this surface inhomogeneity has minimal impact on the biological properties of the scaffolds.[31] The composite hydrogel scaffold exhibits three-dimensional porosity, with a reduced pore size compared to the simple GelMA hydrogel. This modification enhances cell migration and nutrient exchange, thereby providing a suitable microenvironment for cell growth and angiogenesis.[32] Additionally, the Young's modulus was increased, likely due to the robust interfacial bonding forces formed between nHA and GelMA. Specifically, Ca^{2+} ions in the hydroxyapatite formed coordination bonds with the $-NH^{2+}$ groups present in GelMA,[33] while the −COOH groups facilitated the establishment of ionic bonds.[34] This bonding significantly improved the scaffold's ability to efficiently transmit stress and enhance the mechanical properties of the material, thereby preserve the scaffold's integrity during cell recruitment and differentiation.[35] Although the addition of nHA and VEGF improved the scaffold's hydrophilicity, the interaction between nHA and GelMA created a more enduring internal structure. This improved stability decreases the degradation rate of the scaffold, resulting in slower drug release rate. The experimental indicated that the release patterns of Ca^{2+} and VEGF exhibited an initial rapid phase, followed by a prolonged slow-release period. This behavior phenomenon be due to the drugs located on the scaffold's exterior, which initially engage interact with the extracellular matrix, increasing their quick release. In contrast, the drugs trapped in within the scaffold matrix require the gradual breakdown of the hydrogel to achieve for sustained release. Furthermore, both the concentration of nHA and the degree of cross-linking in GelMA influenced the release kinetics of Ca^{2+} and VEGF. Collectively, these combined release mechanisms enhance the scaffold's effectiveness in fostering osteogenesis and angiogenesis during the initial phases of implantation while ensuring adequate concentration of Ca^{2+} and VEGF in the subsequent phases to support the development of bone and vascular structures.

Biocompatibility is the primary criterion for evaluating the suitability of a stent for human.[36] The results indicated that the composite hydrogel scaffold significantly enhanced cell proliferation but did not cause significant changes to the cell morphology. This phenomenon may be due to the three-dimensional porous structure of the scaffold, which provides a relatively confined microenvironment that preserves the cell shape. The presence of the RGD sequence within the GelMA hydrogel improves the binding to receptors on cell surfaces, enhancing the cell adhesion, proliferation and migration. The incorporation of nHA to the scaffold creates a microenvironment similar to that of the bone tissue because of its structural resemblance to the hydroxyapatite found in natural bone. Moreover, nHA acts as a direct adhesion site for cells and stimulates the osteogenic differentiation of BMSCs.[37] Furthermore, the released Ca^{2+} serves as an intracellular secondary messenger which promotes the proliferation and migration of BMSCs.[38] Furthermore, vascular endothelial growth factor (VEGF) interacts with the vascular endothelial growth factor receptor (VEGF-R) located on the cell surface, promoting both cell proliferation and migration.[39] The cell experiments revealed that the composite hydrogel scaffold accelerated the differentiation of BMSCs into osteoblasts. Throughout the differentiation process, the expression levels of osteogenesis-related proteins, such as ALP, OCN and RUNX-2 were significantly increased. Furthermore, BMSCs formed significant calcium nodules 21 days after induction. Integrins located on the surface of BMSCs were attached to the surface of nano-hydroxyapatite (nHA), thereby activating various intracellular signaling pathways, including the mitogen-activated protein kinase (MAPK) signaling pathway.[40] Notably, elevated levels of Ca^{2+} within the extracellular matrix can pass through the cell membrane via Ca^{2+} ion channels, and the subsequent rise in intracellular Ca^{2+}concentration can trigger diverse signaling pathways in BMSCs, including the Wnt signaling pathway[41] and the calmodulin kinase (CaMK) signaling pathway.[42] Activation of these pathways can upregulate the RUNX-2 expression. In addition, the VEGF, which is released during the initial phases of composite hydrogel scaffold interaction to promote RUNX-2 expression,[43] further amplifying RUNX-2 levels through the synergistic effect of $Ca^{2+}$and VEGF interaction. RUNX-2 is an important transcription factor that influences the differentiation of mesenchymal stem cells into osteoblasts. Increased RUNX-2 levels have been reported to promote the expression of alkaline phosphatase (ALP)[44] and osteocalcin (OCN)[45] enhancing the bone tissue mineralization. In the initial phases of bone healing, the levels of RUNX-2 and OCN increased in all experimental groups, which is consistent with the observations of the cell experiments. Conversely, in the subsequent phases of bone healing, the composite hydrogel scaffold group had decreased levels of RUNX-2, whereas OCN levels continued to be high. This finding may imply that as the healing process of bone

progresses, osteoblasts gradually transition into osteocytes, resulting in a slow decline of RUNX-2 levels. The OCN, a protein released by osteoblasts, plays a crucial role in the later phases of osteogenesis and bone mineralization, by controlling calcium, phosphorus, and other mineral deposits in the bone matrix. The mineralization of bone is accelerated by the combined effects of high concentrations of Ca^{2+} and VEGF within cells, improving the recovery of bone defect regions. The composite hydrogel scaffold releases calcium ions while simultaneously releasing phosphate ions. The localized high concentration of phosphate ions can promote the formation of collagen fibers,[46] which enhances the ability of these fibers to capture additional calcium ions and improves the amorphous phosphate through interface control. The infiltration of calcium into the collagen further enhances the interaction between the inorganic mineral ions and the collagen matrix, thereby regulating the mineralization of collagen fibers.[47] This suggests that the composite hydrogel stents designed in this study effectively promoted bone healing.

The restoration of bone tissue should occur parallel with that of the vascular network, which is a considerable challenge in the realm of bone tissue engineering.[48] In this research, we employed nHA and GelMA as delivery systems for VEGF to improve vascularization within bone defect regions. Although ultraviolet irradiation affects protein structure, VEGF can retain its biological activity under short-term and low-intensity ultraviolet exposure.[49] We employed the ELISA method to measure the release of VEGF in the composite hydrogel. In vitro experiments revealed that CD31 expression in BMSCs within the composite hydrogel scaffold group was significantly increased, indicating that the composite hydrogel scaffold promotes the endothelial differentiation of BMSCs and enhances the ability of HUVECs to form tubes. At four weeks, a higher quantity of blood vessels was formed in the group treated with the composite hydrogel scaffold, accompanied with increased blood flow, as indicated by laser speckle blood flow imaging and histological examinations. Moreover, blood vessels were seen growing inward from the surface of the scaffold, highlighting that the scaffold improved angiogenesis. However, when we performed the same evaluation at eight weeks, the composite hydrogel scaffold group had the lowest levels of blood flow, and the expression of α-SMA was lowest in the examined sections. This reduction may be attributed to the early formation of a substantial number of new blood vessels within this group, which likely enhanced blood circulation and accelerated bone healing. During the repair of fractures, some of these newly formed blood vessels undergo remodeling, which causes decreases the overall number of vessels. The Ca^{2+} ions released during the breakdown of the composite hydrogel scaffold can penetrate endothelial cells via calcium ion channels. Ca^{2+} functions as an intracellular second messenger, influencing the phosphorylation of VEGF-R[48] and improving its interaction with VEGF released from the scaffold. The increase in VEGF subsequently promotes endothelial cell proliferation, migration, lumen formation, and other processes associated with vascular regeneration. In summary, the synergistic effects of Ca^{2+} and VEGF endowed the scaffold with the ability to form blood vessel, thereby enhancing bone healing. However, the high cost of VEGF has consistently limited its use. In this study, we significantly extended the sustained release time of VEGF through a GelMA-nHA hydrogel precise sustained release system,[50] thereby improving the utilization rate of VEGF. A single implantation can continuously promote angiogenesis and bone regeneration. In the future, the integration of gene editing technology or the development of composite hydrogel peptides with gene editing may help reduce costs while maintaining efficacy, offering a new pathway for clinical transformation.

This study has certain limitations. While our composite hydrogel stent effectively promotes the synergistic effects of vascular and bone regeneration in skull defects in rats, its application in the weight-bearing areas of larger animals may present challenges. This is primarily because materials used in these areas must possess superior mechanical properties. Previous research has demonstrated that increasing the concentration of nHA and utilizing 3D printing technology can significantly enhance the mechanical properties of materials.[51] Consequently, we can refine the synthesis process of these materials through 3D printing technology to improve their mechanical properties, thereby facilitating their application in promoting vascular and bone regeneration in the bone defect areas of larger animals. This approach will provide a more robust foundation for future clinical applications.

Conclusion

In summary, we propose a composite hydrogel scaffold that utilizes GelMA matrix with favorable properties including enhanced cell adhesion. The incorporation of nHA further improves the mechanical strength of the scaffold. Additionally, calcium ions released from the scaffold bind to VEGF, promoting angiogenesis and bone formation The present results

indicate that the composite scaffold increases the expression levels of ALP, ARS, OCN, RUNX-2 and CD31 thereby facilitating the osteogenic differentiation of BMSCs and enhancing the tube-forming capacity of HUVECs. Moreover, the composite hydrogel stents effectively promotes vascular and bone regeneration in critical-sized skull defects in rats, accelerating the healing process in the affected area. Although composite hydrogel stents exhibit good biocompatibility, they are still recognized as foreign bodies by the host, and their potential to induce sterile inflammatory responses remains to be evaluated. Furthermore, the drug release characteristics of implanted stents, along with their degradation and mineralization properties, have not been thoroughly analyzed. Additional studies are warranted to investigate the detailed performance of the scaffold.

Abbreviations

GelMA, Gelatin methacryloyl; HA, Hydroxyapatite; nHA, Nanohydroxyapatite; VEGF, vascular endothelial growth factor; HUVEC, human umbilical vein endothelial cells; BMSC, bone marrow mesenchymal stem cells; MMPs, matrix metalloproteinases; FBS, Fetal bovine serum; ALP, Alkaline phosphatase; ARS, alizarin red staining; OCN, osteocalcin; RUNX-2, Runt-related transcription factor 2; CD31, Platelet endothelial cell adhesion molecule-1; α-SMA, α-smooth muscle actin.

Data Sharing Statement

The data that support the findings of this study are available from the corresponding author upon reasonable request.

Ethics Approval

The experimental procedure followed the United States National Institutes of Health Guide for the Care and Use of Laboratory Animals (NIH Publication No. 85–23, revised 1985). The study protocol was approved by the Animal Ethics Committee of Bengbu Medical College (approval number: 2023[485]).

Acknowledgments

This study was supported by the Natural Science Research Project of the Anhui Education Committee (KJ2021A0723), the key projects of Anhui Provincial Health Commission. (AHWJ2023A10086).

Author Contributions

All authors made a significant contribution to the work reported, whether that is in the conception, study design, execution, acquisition of data, analysis and interpretation, or in all these areas; took part in drafting, revising or critically reviewing the article; gave final approval of the version to be published; have agreed on the journal to which the article has been submitted; and agree to be accountable for all aspects of the work.

Disclosure

The authors declare no competing interests in this work.

References

1. Kusumbe AP, Ramasamy SK, Adams RH. Coupling of angiogenesis and osteogenesis by a specific vessel subtype in bone. *Nature*. 2014;507(7492):323–328. doi:10.1038/nature13145
2. Bi M, Yang K, Yu T, Wu G, Li Q. Cell-based mechanisms and strategies of co-culture system both in vivo and vitro for bone tissue engineering. *Biomed Pharmacother*. 2023;169:115907. doi:10.1016/j.biopha.2023.115907
3. Bosch-Rue E, Diez-Tercero L, Buitrago JO, Castro E, Perez RA. Angiogenic and immunomodulation role of ions for initial stages of bone tissue regeneration. *Acta Biomater*. 2023;166:14–41. doi:10.1016/j.actbio.2023.06.001
4. Akita S, Tamai N, Myoui A, et al. Capillary vessel network integration by inserting a vascular pedicle enhances bone formation in tissue-engineered bone using interconnected porous hydroxyapatite ceramics. *Tissue Eng*. 2004;10(5–6):789–795. doi:10.1089/1076327041348338
5. Yuan Q, Li L, Peng Y, et al. Biomimetic nanofibrous hybrid hydrogel membranes with sustained growth factor release for guided bone regeneration. *Biomater Sci*. 2021;9(4):1256–1271. doi:10.1039/d0bm01821j
6. Zhang M, Matinlinna JP, Tsoi JKH, et al. Recent developments in biomaterials for long-bone segmental defect reconstruction: a narrative overview. *J Orthop Translat*. 2020;22:26–33. doi:10.1016/j.jot.2019.09.005

7. Burger MG, Grosso A, Briquez PS, et al. Robust coupling of angiogenesis and osteogenesis by VEGF-decorated matrices for bone regeneration. *Acta Biomater*. 2022;149:111–125. doi:10.1016/j.actbio.2022.07.014
8. Chen S, Cheng D, Bao W, et al. Polydopamine-functionalized strontium alginate/hydroxyapatite composite microhydrogel loaded with vascular endothelial growth factor promotes bone formation and angiogenesis. *ACS Appl Mater Interfaces*. 2024;16(4):4462–4477. doi:10.1021/acsami.3c16822
9. Ferrara N. Vascular endothelial growth factor: basic science and clinical progress. *Endocr Rev*. 2004;25(4):581–611. doi:10.1210/er.2003-0027
10. Zhang M, Yu W, Niibe K, et al. The effects of platelet-derived growth factor-BB on bone marrow stromal cell-mediated vascularized bone regeneration. *Stem Cells Int*. 2018;2018:3272098. doi:10.1155/2018/3272098
11. Stegen S, van Gastel N, Carmeliet G. Bringing new life to damaged bone: the importance of angiogenesis in bone repair and regeneration. *Bone*. 2015;70:19–27. doi:10.1016/j.bone.2014.09.017
12. Hausman MR, Schaffler MB, Majeska RJ. Prevention of fracture healing in rats by an inhibitor of angiogenesis. *Bone*. 2001;29(6):560–564. doi:10.1016/s8756-3282(01)00608-1
13. Wang S, Duan C, Yang W, et al. Two-dimensional nanocoating-enabled orthopedic implants for bimodal therapeutic applications. *Nanoscale*. 2020;12(22):11936–11946. doi:10.1039/d0nr02327b
14. Hu K, Olsen BR. Osteoblast-derived VEGF regulates osteoblast differentiation and bone formation during bone repair. *J Clin Invest*. 2016;126(2):509–526. doi:10.1172/JCI82585
15. Wang Y, Wan C, Deng L, et al. The hypoxia-inducible factor alpha pathway couples angiogenesis to osteogenesis during skeletal development. *J Clin Invest*. 2007;117(6):1616–1626. doi:10.1172/JCI31581
16. Barati D, Shariati SRP, Moeinzadeh S, Melero-Martin JM, Khademhosseini A, Jabbari E. Spatiotemporal release of BMP-2 and VEGF enhances osteogenic and vasculogenic differentiation of human mesenchymal stem cells and endothelial colony-forming cells co-encapsulated in a patterned hydrogel. *J Control Release*. 2016;223:126–136. doi:10.1016/j.jconrel.2015.12.031
17. Raina DB, Liu Y, Isaksson H, Tagil M, Lidgren L. Synthetic hydroxyapatite: a recruiting platform for biologically active molecules. *Acta Orthop*. 2020;91(2):126–132. doi:10.1080/17453674.2019.1686865
18. Munir MU, Salman S, Javed I, et al. Nano-hydroxyapatite as a delivery system: overview and advancements. *Artif Cells Nanomed Biotechnol*. 2021;49(1):717–727. doi:10.1080/21691401.2021.2016785
19. Shuai C, Peng B, Feng P, Yu L, Lai R, Min A. In situ synthesis of hydroxyapatite nanorods on graphene oxide nanosheets and their reinforcement in biopolymer scaffold. *J Adv Res*. 2022;35:13–24. doi:10.1016/j.jare.2021.03.009
20. Shuai C, Shi X, Wang K, Gu Y, Yang F, Feng P. Ag-doped CNT/HAP nanohybrids in a PLLA bone scaffold show significant antibacterial activity. *Bio-Des Manuf*. 2024;7:105–120. doi:10.1007/s42242-023-00264-0
21. Shuai C, Yang W, Feng P, Peng S, Pan H. Accelerated degradation of HAP/PLLA bone scaffold by PGA blending facilitates bioactivity and osteoconductivity. *Bioact Mater*. 2021;6(2):490–502. doi:10.1016/j.bioactmat.2020.09.001
22. Douglas TEL, Schietse J, Zima A, et al. Novel self-gelling injectable hydrogel/alpha-tricalcium phosphate composites for bone regeneration: physiochemical and microcomputer tomographical characterization. *J Biomed Mater Res A*. 2018;106(3):822–828. doi:10.1002/jbm.a.36277
23. Baines DK, Wright K, Douglas TEL. Preliminary in vitro assessment of whey protein isolate hydrogel with cannabidiol as a potential hydrophobic oral drug delivery system for colorectal cancer therapy. *Polymers*. 2024;16(23):3273. doi:10.3390/polym16233273
24. Wang J, Wang X, Liang Z, et al. Injectable antibacterial Ag-HA/ GelMA hydrogel for bone tissue engineering. *Front Bioeng Biotechnol*. 2023;11:1219460. doi:10.3389/fbioe.2023.1219460
25. Wu Y, Fu R, Mohanty S, Nasser M, Guo B, Ghosh G. Investigation of integrated effects of hydroxyapatite and VEGF on capillary morphogenesis of endothelial cells. *ACS Appl Bio Mater*. 2019;2(6):2339–2346. doi:10.1021/acsabm.8b00780
26. Celikkin N, Mastrogiacomo S, Jaroszewicz J, Walboomers XF, Swieszkowski W. Gelatin methacrylate scaffold for bone tissue engineering: the influence of polymer concentration. *J Biomed Mater Res A*. 2018;106(1):201–209. doi:10.1002/jbm.a.36226
27. Lu W, Zeng M, Liu W, et al. Human urine-derived stem cell exosomes delivered via injectable GelMA templated hydrogel accelerate bone regeneration. *Mater Today Bio*. 2023;19:100569. doi:10.1016/j.mtbio.2023.100569
28. Huang S, Wang Z, Sun X, Li K. Bone morphogenetic protein 7-loaded gelatin methacrylate/oxidized sodium alginate/nano-hydroxyapatite composite hydrogel for bone tissue engineering. *Int J Nanomed*. 2024;19:6359–6376. doi:10.2147/IJN.S461996
29. Zeimaran E, Pourshahrestani S, Fathi A, et al. Advances in bioactive glass-containing injectable hydrogel biomaterials for tissue regeneration. *Acta Biomater*. 2021;136:1–36. doi:10.1016/j.actbio.2021.09.034
30. Gaharwar AK, Peppas NA, Khademhosseini A. Nanocomposite hydrogels for biomedical applications. *Biotechnol. Bioeng*. 2013;111(3):441–453. doi:10.1002/bit.25160
31. Šupová M. Problem of hydroxyapatite dispersion in polymer matrices: a review. *J Mater Sci Mater Med*. 2009;20(6):1201–1213. doi:10.1007/s10856-009-3696-2
32. Wang Q, Zhang Y, Li B, Chen L. Controlled dual delivery of low doses of BMP-2 and VEGF in a silk fibroin-nanohydroxyapatite scaffold for vascularized bone regeneration. *J Mater Chem B*. 2017;5(33):6963–6972. doi:10.1039/c7tb00949f
33. Liu Y, Wang C, Xue J, et al. Body temperature enhanced adhesive, antibacterial, and recyclable ionic hydrogel for epidermal electrophysiological monitoring. *Adv Healthc Mater*. 2022;11(15):e2200653. doi:10.1002/adhm.202200653
34. Liang K, Spiesz EM, Schmieden DT, Xu A-W, Meyer AS, Aubin-Tam M-E. Bioproduced polymers self-assemble with graphene oxide into nanocomposite films with enhanced mechanical performance. *ACS Nano*. 2020;14(11):14731–14739. doi:10.1021/acsnano.0c00913
35. Wang Q, Brächer T, Mohseni M, et al. Nanoscale spin-wave wake-up receiver. *Appl Phys Lett*. 2019;115. doi:10.1063/1.5109623
36. Gao X, Xu Z, Li S, et al. Chitosan-vancomycin hydrogel incorporated bone repair scaffold based on staggered orthogonal structure: a viable dually controlled drug delivery system. *RSC Adv*. 2023;13(6):3759–3765. doi:10.1039/d2ra07828g
37. Makar LE, Nady N, Abd El-Fattah A, Shawky N, Kandil SH. Unmodified gum Arabic/chitosan/nanohydroxyapatite nanocomposite hydrogels as potential scaffolds for bone regeneration. *Polymers*. 2022;14(15):3052. doi:10.3390/polym14153052
38. Lee MN, Hwang HS, Oh SH, et al. Elevated extracellular calcium ions promote proliferation and migration of mesenchymal stem cells via increasing osteopontin expression. *Exp mol Med*. 2018;50(12):1–16. doi:10.1038/s12276-018-0170-6
39. Beamer B, Hettrich C, Lane J. Vascular endothelial growth factor: an essential component of angiogenesis and fracture healing. *HSS J*. 2010;6(1):85–94. doi:10.1007/s11420-009-9129-4

40. Li W, Huang C, Ma T, et al. Low-frequency electromagnetic fields combined with tissue engineering techniques accelerate intervertebral fusion. *Stem Cell Res Ther*. 2021;12(1):143. doi:10.1186/s13287-021-02207-x
41. Gao Y, Chen N, Fu Z, Zhang Q. Progress of Wnt signaling pathway in osteoporosis. *Biomolecules*. 2023;13(3):483. doi:10.3390/biom13030483
42. Wang B, Shao W, Zhao Y, et al. Radial extracorporeal shockwave promotes osteogenesis-angiogenesis coupling of bone marrow stromal cells from senile osteoporosis via activating the Piezo1/CaMKII/CREB axis. *Bone*. 2024;187:117196. doi:10.1016/j.bone.2024.117196
43. Zhang M, Fukushima Y, Nozaki K, et al. Enhancement of bone regeneration by coadministration of angiogenic and osteogenic factors using messenger RNA. *Inflamm Regen*. 2023;43(1):32. doi:10.1186/s41232-023-00285-3
44. Darjanki CM, Prahasanti C, Fitria AE, Kusumawardani B, Wijaksana IKE, Aljunaid M. RUNX2 and ALP expression in osteoblast cells exposed by PMMA-HAp combination: an in vitro study. *J Oral Biol Craniofacial Res*. 2023;13(2):277–282. doi:10.1016/j.jobcr.2023.02.007
45. Yao H, Zou Y, Yang K, Yin L, Liu Y, Li R. TGFβ1 induces bone formation from BMP9-activated bone mesenchymal stem cells, with possible involvement of non-canonical pathways. *Int J Med Sci*. 2020;17(12):1692–1703. doi:10.7150/ijms.45786
46. Meng D, Li W, Ura K, Takagi Y. Effects of phosphate ion concentration on in-vitro fibrillogenesis of sturgeon type I collagen. *Int J Biol Macromol*. 2020;148:182–191. doi:10.1016/j.ijbiomac.2020.01.128
47. Zheng B, Zhao L, Chen L, et al. Phosphorylation of collagen fibrils enhances intrafibrillar mineralization and dentin remineralization. *Nanoscale*. 2024;16(24):11633–11641. doi:10.1039/d4nr00652f
48. Man XY, Yang XH, Cai SQ, Bu ZY, Zheng M. Overexpression of vascular endothelial growth factor (VEGF) receptors on keratinocytes in psoriasis: regulated by calcium independent of VEGF. *J Cell & mol Med*. 2007;12(2):649–660. doi:10.1111/j.1582-4934.2007.00112.x
49. Schuurman W, Levett PA, Pot MW, et al. Gelatin-methacrylamide hydrogels as potential biomaterials for fabrication of tissue-engineered cartilage constructs. *Macromol Biosci*. 2013;13(5):551–561. doi:10.1002/mabi.201200471
50. Ding S, He S, Ye K, Shao X, Yang Q, Yang G. Photopolymerizable, immunomodulatory hydrogels of gelatin methacryloyl and carboxymethyl chitosan as all-in-one strategic dressing for wound healing. *Int J Biol Macromol*. 2023;253(Pt 6). doi:10.1016/j.ijbiomac.2023.127151
51. Wang H, Li X, Lai S, et al. Construction of vascularized tissue engineered bone with nHA-coated BCP bioceramics loaded with peripheral blood-derived MSC and EPC to repair large segmental femoral bone defect. *ACS Appl Mater Interfaces*. 2022;15(1):249–264. doi:10.1021/acsami.2c15000